Supporting information:

1) Experimental methods

$Nd_{⅓}NbO_3$ was prepared by solid state reactions as described previously.[7] Stoichiometric amounts of Nd_2O_3 and Nb_2O_5 were ground intimately in an agate pestle and mortar. The sample was then pressed as a pellet and heated at 1000˚C for 12 h and then 1300˚C for 12 h several times (with intermittent grinding) to prepare $Nd_{⅓}NbO_3$.

For reductive lithiation reactions, a solid $Nd_{⅓}NbO_3$ (2g, 10.6 mmol) was transferred into a Schlenk flask and placed under vacuum for 1 minute to degas, after which the flask was refilled with Ar and nBuLi (80 cm^3, 1.6 M in hexanes, 128 mmol) added to the the stirring solid, forming a dark blue suspension which was stirred at ambient temperature for a week. The solid was isolated by filtration, washed with nHexane (10 cm^3), and dried under vacuum to give $Li_xNd_{⅓}NbO_3$ as a dark blue, air-sensitive solid which oxidises in air in minutes to give a grey solid. For lithiation reactions, nHexane was distilled from Na/Benzophenone bfore use and stored over 4 Å sieves under argon. BuLi was purchased from Fisher Scientific and used as supplied. $Li_xNd_{⅓}NbO_3$ prepared was contaminated with colourless crystals and these were separated from the product by Pasteur separation in an argon-filled glovebox.

$Nd_{1/3}NbO_3$ and $Li_xNd_{⅓}NbO_3$ were characterised by XRPD using a Rigaku Miniflex with Cu Ka radiation (40 kV, 15 mA) and a D/teX Ultra detector. (Data for $Li_xNd_{⅓}NbO_3$ were collected using an air-sensitive sample holder). Low temperature XRPD data were collected using a PANalytical Empyrean diffractometer (with a Ge monochromator, an X'Celerator detector and an Oxford Cryosystems Phenix Cryostat). NPD data were collected on both samples at the high resolution HRPD diffractometer at the ISIS neutron and muon source (Rutherford Appleton Lab, U.K.) via the HRPD Xpress route. Samples were loaded into cylindrical 6 mm diameter vanadium cans ($Li_xNd_{⅓}NbO_3$ was loaded in an Ar-filled glovebox and sealed with indium wire; lithium of natural abundance was used). Data were collected at room temperature in HRPD's 30-130 ms window and data were corrected for absorption. Rietveld refinement[1] was carried out using TopasAcademic[2-3] or Jana[4] and ISODISTORT[5] was used to consider possible structural distortions. Field-cooled (FC) and zero-field-cooled (ZFC) magnetisation was measured on warming in an applied field of 1000 Oe using a QD MPMS. The first principles calculations of the effective A^{2+} models were performed using the VASP[6-7] and ABINIT packages;[8] both employed the PBEsol[9] exchange correlation functional and PAW pseudopotentials. The plane wave cutoff was set to 1000 eV and we used a 5×5×3 *k*-point mesh for the 18 atom cell, which was scaled proportionally for other size cells (see SI).

Iodometric titrations to determine lithium content were carried out. A solution of I2 (217 mg, 8.5×10^{-4} moles) in dry acetonitrile (15 ml) were added to $Li_xNd_{⅓}NbO_3$ (0.3 g, 1.57×10^{-3} moles) under Ar and left to stir under Ar for 12 hours. The resulting solution was diluted to 50 cm^3 and titrated with $Na_2S_2O_3$ (0.02 M) (back titration) using a starch indicator to identify the end-point.

2) Nd⅓NbO$_3$: broadening of superstructure reflections in high resolution NPD data

Compared with the diffraction pattern expected for the ideal high symmetry *P*4/*mmm* aristotype structure, additional reflections are observed in room temperature NPD data for Nd⅓NbO$_3$ that indicate a doubling of the unit cell along [100] and [010] directions, and a noticeable orthorhombic distortion. Figure SI2.1. shows the fit to an orthorhombic Pawley phase with $a \approx b \approx a_p$ and $c \approx c_p$, clearly highlighting broadened superstructure reflections not fitted by this smaller unit cell.

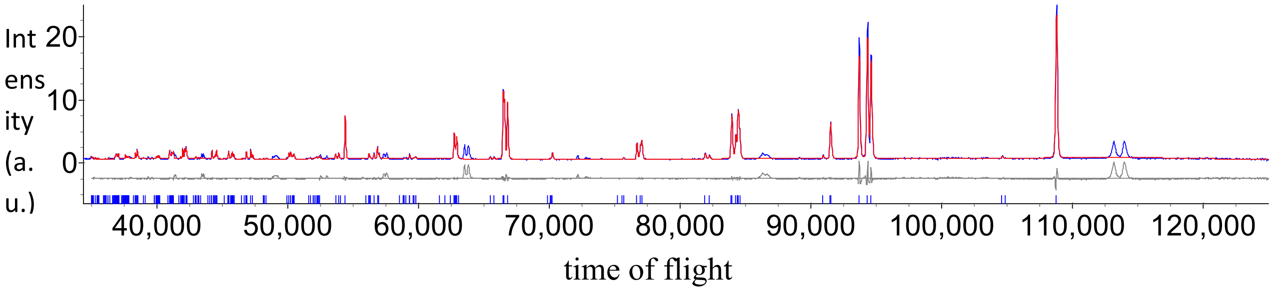

Figure SI2.1 Refinement profiles for Pawley phase of *P*222 symmetry (a = 3.9072(1) Å, b = 3.8813(1) Å, c = 7.8388(2) Å) to fit room temperature NPD data (showing only the highest resolution 168° bank of data) collected for Nd⅓NbO$_3$ showing observed, calculated and difference profiles in blue, red and grey, respectively, with peak positions shown by blue ticks. Pairs of superstructure reflections are clearly observed at 113800 μs, 64000 μs and 58000 μs, for example.

The *Cmmm* model reported by Zhou et al[10] fits these data relatively well, although the profile of these superstructure reflections isn't well fitted (Figure SI2.2).

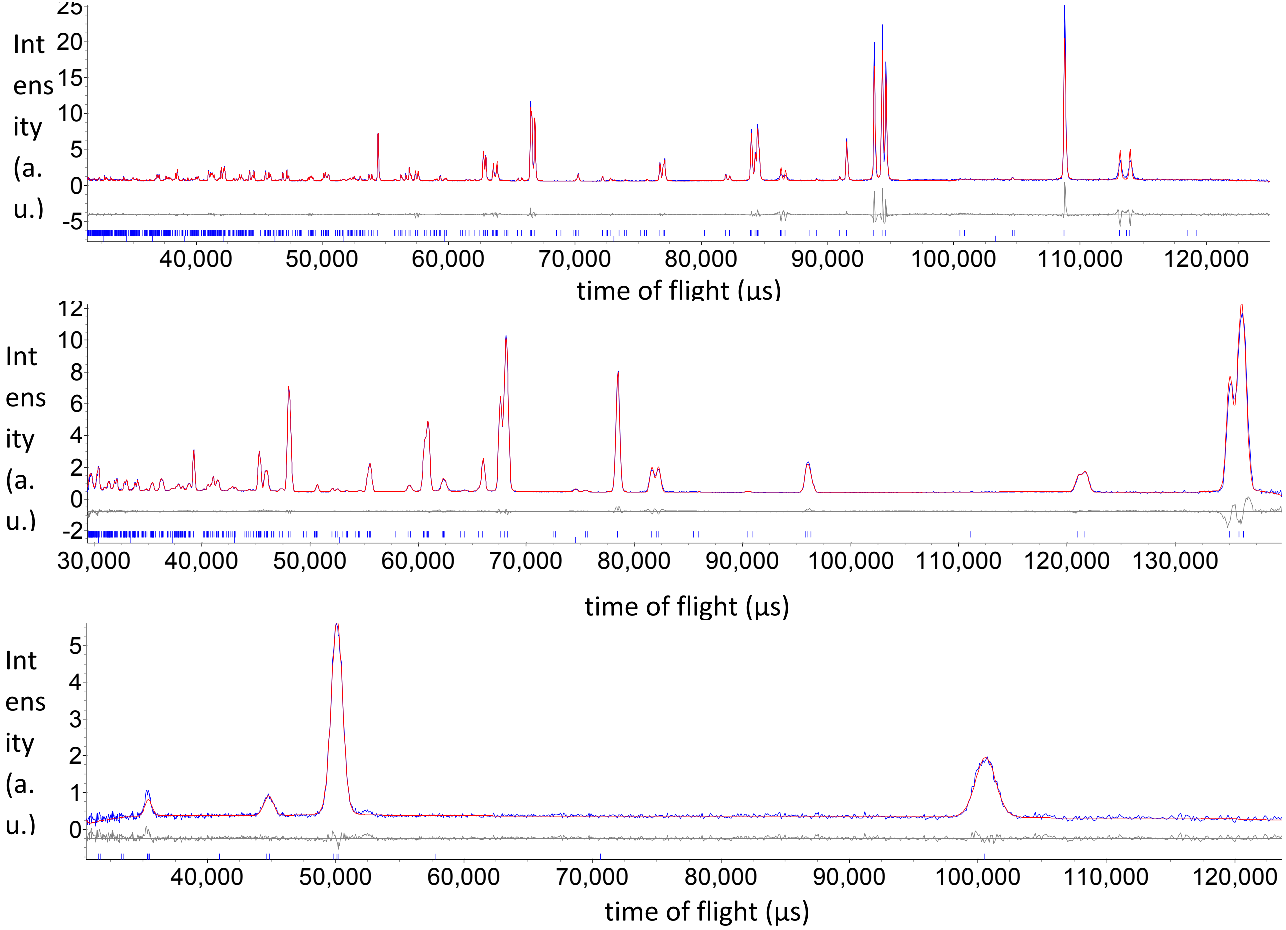

Figure SI2.2 Rietveld refinement profiles for room temperature NPD data collected for Nd⅓NbO$_3$ with *Cmmm* model (with no broadening of superstructure reflections) showing observed, calculated and difference profiles in blue, red and grey, respectively, with peak positions shown by blue ticks; R_{wp} = 4.45%, R_p = 5.51% and χ^2 = 4.47. The upper panel shows the fit to the highest resolution backscattered bank, in the middle the 90° bank of data and bottom, lowest resolution 30° bank of data.

The fit is improved significantly if a size-dependent broadening term is applied to the superstructure reflections (Figure SI2.3), suggesting a correlation length of $a^-b^0c^0$ tilts of ~50 Å.

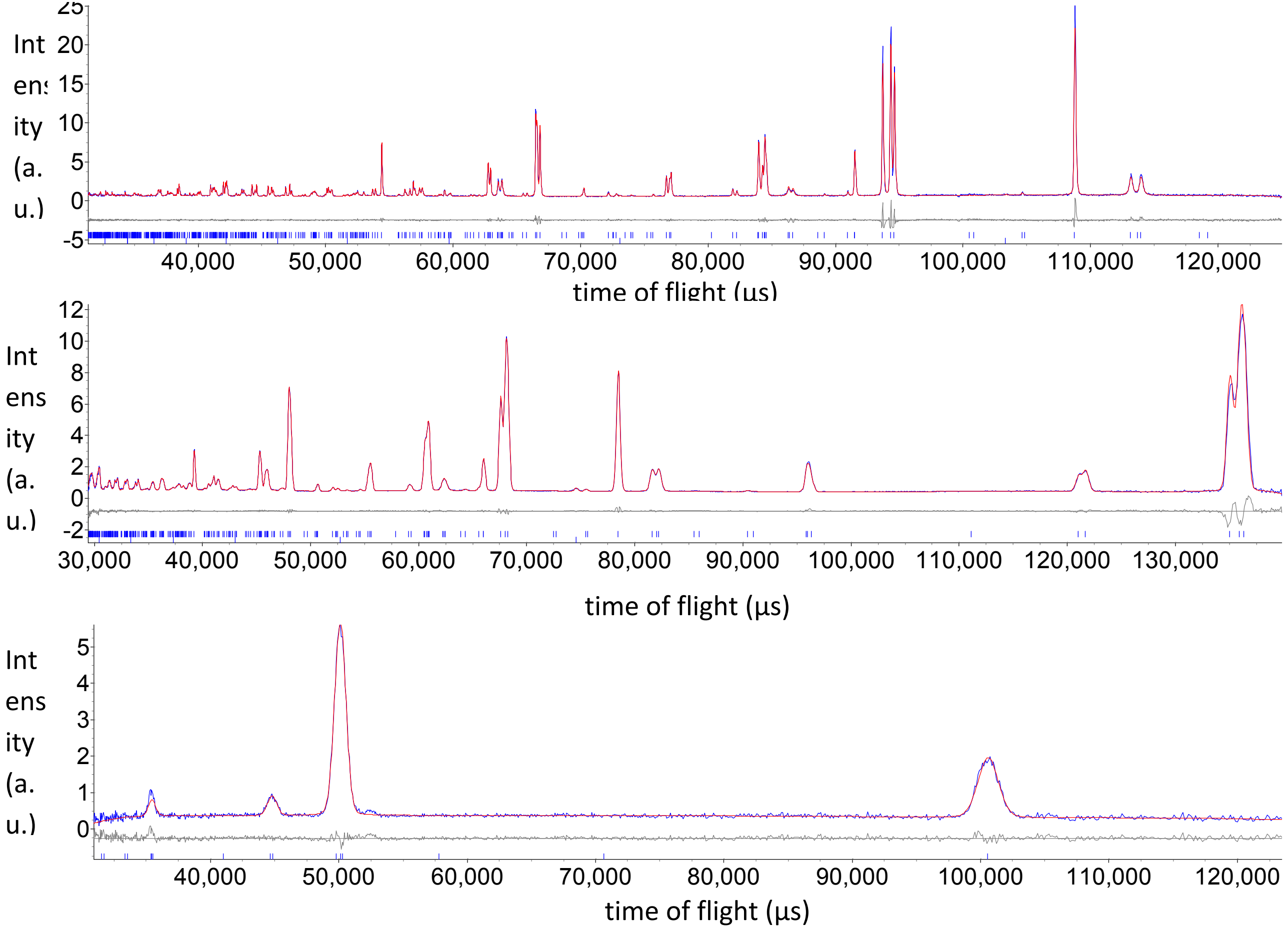

Figure SI2.3 Rietveld refinement profiles for room temperature NPD data collected for Nd$_{2/3}$NbO$_3$ with *Cmmm* model (with broadening of superstructure reflections) showing observed, calculated and difference profiles in blue, red and grey, respectively, with peak positions shown by blue ticks; R_{wp} = 3.49%, R_p = 4.68% and χ^2 = 2.75. The upper panel shows the fit to the highest resolution backscattered bank, in the middle the 90° bank of data and bottom, lowest resolution 30° bank of data.

Table SI2.1 Refinement details and selected bond lengths from Rietveld refinements using room temperature NPD data collected for Nd$_{2/3}$NbO$_3$ with *Cmmm* model with *a* = 7.8144(5) Å, *b* = 7.76249(5) Å, *c* = 7.83859(5) Å, volume = 475.482(6) Å^3.

Atom	**site**	**x**	**y**	**z**	**occupancy**
Nd	4g	0.2547(2)	0	0	0.667
Nb	8n	0	0.2482(2)	0.2609(1)	1
O(1)	4i	0	0.2878(2)	0	1
O(2)	4j	0	0.2128(1)	0.5	1
O(3)	4k	0	0	0.2010(1)	1
O(4)	4l	0	0.5	0.2725(1)	1
O(5)	8m	0.25	0.25	0.2302(1)	1

	U_{ij} × 100 (Å^2)					
Atom	**U_{11}**	**U_{22}**	**U_{33}**	**U_{12}**	**U_{13}**	**U_{23}**
Nd	0.8(1)	0.49(8)	0.82(1)	0.08(9)	0	0
Nb	1.12(4)	0.99(3)	1.56(5)	0	0	0.20(3)
O(1)	3.4(1)	1.7(1)	0.32(6)	0.9(1)	0	0
O(2)	3.5(1)	0.6(1)	0.74(7)	0.1(1)	0	0
O(3)	1.4(1)	0.01(9)	0.9(1)	0	0.6(1)	0
O(4)	4.7(2)	0.9(1)	0.9(1)	0	0.0(1)	0
O(5)	0.44(4)	2.80(5)	3.77(7)	-0.2(1)	0	0

Bond	Length (Å)	Bond	Length (Å)
Nd – O(1)	2 × 2.527(2)	Nb – O(2)	1.8943(8)
Nd – O(1)	2 × 2.992(2)	Nb – O(4)	1.957(1)
Nd – O(3)	2 × 2.539(2)	Nb – O(5)	2 × 1.9684(1)
Nd – O(5)	4 × 2.6500(8)	Nb – O(3)	1.983(1)
Nd – O(4)	2 × 2.870(1)	Nb – O(1)	2.0680(8)

Allowing further distortions of the structural model for $Nd_{1/3}NbO_3$ to include $a^-b^0c^+$ tilts lowers the symmetry to *C*2*mm* (non-standard setting of *Amm*2). With only a very slight improvement in fit (Figure SI2.4, Table SI2.4), and in the absence of any polar property measurements, it seems reasonable to assume the centrosymmetric *Cmmm* model at room temperature, at least at the length scale probed by long-range diffraction measurements.

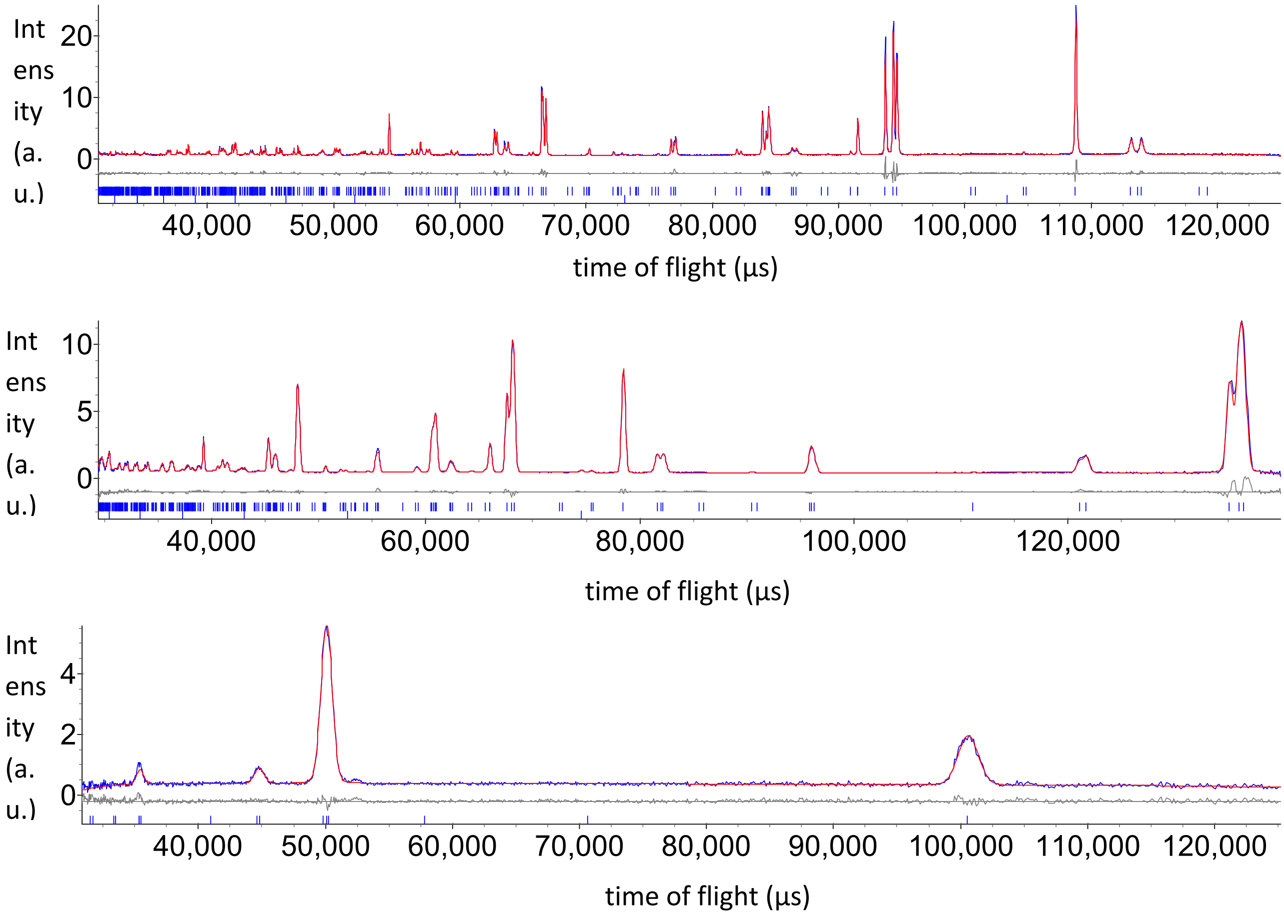

Figure SI2.4 Rietveld refinement profiles for room temperature NPD data collected for $Nd_{1/3}NbO_3$ with *C2mm* model (with broadening of superstructure reflections) showing observed, calculated and difference profiles in blue, red and grey, respectively, with peak positions shown by blue ticks; R_{wp} = 5.00%, R_p = 5.46% and χ^2 = 5.65. The upper panel shows the fit to the highest resolution backscattered bank, in the middle the 90° bank of data and bottom, lowest resolution 30° bank of data.

Table SI2.4 Refinement details and selected bond lengths from Rietveld refinements using room temperature NPD data collected for $Nd_{1/3}NbO_3$ with *C*2*mm* model with *a* = 7.76251(7) Å, *b* = 7.81443(7) Å, *c* = 7.83863(8) Å, volume 475.488(8) Å^3.

Atom	site	*x*	*y*	*z*	occupancy	U_{iso} × 100 (Å^2)
Nd	4*d*	0.752(1)	0.7463(3)	0	0.667	0.73(4)
Nb(1)	4*c*	0*	0	0.2633(8)	1	1.4(1)
Nb(2)	4*c*	0.5007(7)	0	0.2573(7)	1	0.6(1)
O(1)	2*a*	0.050(1)	0	0	1	1.5(2)
O(2)	2*a*	0.474(1)	0	0	1	1.7(2)
O(3)	2*b*	-0.030(1)	0	0.5	1	1.9(2)
O(4)	2*b*	0.543(1)	0	0.5	1	1.4(2)
O(5)	4*c*	0.752(1)	0	0.1995(2)	1	1.06(6)
O(6)	4*c*	0.251(1)	0	0.2735(2)	1	1.51(6)
O(7)	8*f*	0.0098(9)	0.251(1)	0.7711(1)	1	2.11(5)

Bond	Length (Å)	Bond	Length (Å)
Nd – O(1)	1 × 2.48(1)	Nb(1) – O(1)	1 × 2.100(7)
Nd – O(1)	1 × 3.04(1)	Nb(1) – O(3)	1 × 1.869(6)
Nd – O(2)	1 × 2.58(1)	Nb(1) – O(5)	1 × 1.99(1)
Nd – O(2)	1 × 2.93(1)	Nb(1) – O(6)	1 × 1.95(1)
Nd – O(5)	2 × 2.525(3)	Nb(1) – O(7)	2 × 1.98(1)
Nd – O(6)	2 × 2.881(2)	Nb(2) – O(2)	1 × 2.028(6)
Nd – O(7)	2 × 2.60(1)	Nb(2) – O(4)	1 × 1.930(6)
Nd – O(7)	2 × 2.69(1)	Nb(2) – O(5)	1 × 2.004(1)
		Nb(2) – O(6)	1 × 1.94(1)
		Nb(2) – O(7)	2 × 1.96(1)

3) Variable temperature X-ray powder diffraction (XRPD) results for $Nd_{1/3}NbO_3$ and for $Li_xNd_{1/3}NbO_3$

XRPD data were collected for both samples at 12 K and on warming. There was no obvious change in crystal structure between 12 K and 300 K from XRPD data (no clear change in diffraction patterns, and no discontinuities in unit cell parameters from sequential Rietveld refinements). However, we note that XRPD data are relatively insensitive to the position of light atoms such as oxygen (and lithium) and as such, we can't rule out a structural phase transition primarily involving a change in octahedral tilts in this temperature range.

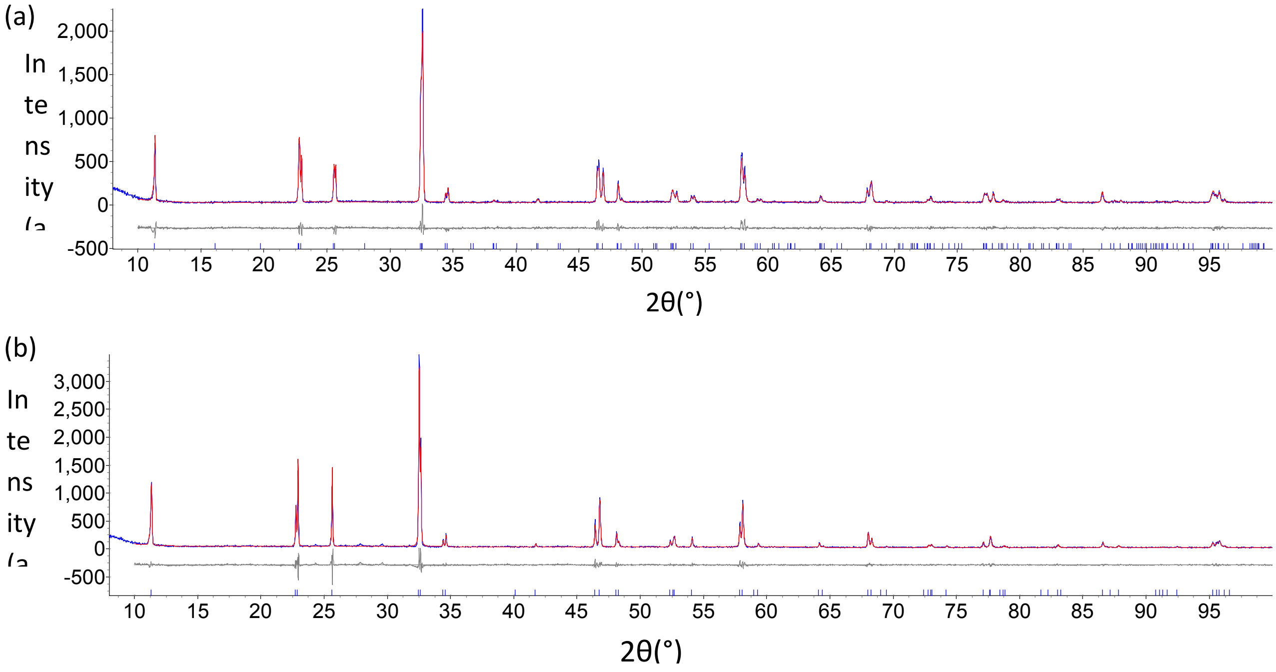

Figure SI3.1 Refinement profiles for 12 K XRPD data collected for (a) $Nd_{1/3}NbO_3$ with *Cmmm* model and (b) $Li_xNd_{1/3}NbO_3$ with *P*4/*mmm* Pawley phase showing observed, calculated and difference profiles in blue, red and grey, respectively, and peak positions shown by blue ticks. 12 K unit cell parameters are a =

7.7530(1) Å, b = 7.8024(1) Å, c = 7.8228(1) Å (*Cmmm* model; R_{wp} = 15.15%, R_p = 11.92% and χ^2 = 1.16) for $\mathrm{Nd}_{1/3}\mathrm{NbO}_3$; *a* = *b* = 3.88319(5) Å, *c* = 7.8234(1) Å (*P4/mmm* Pawley phase; R_{wp} = 16.04%, R_p = 12.19% and χ^2 = 1.48) for $\mathrm{Li}_x\mathrm{Nd}_{1/3}\mathrm{NbO}_3$.

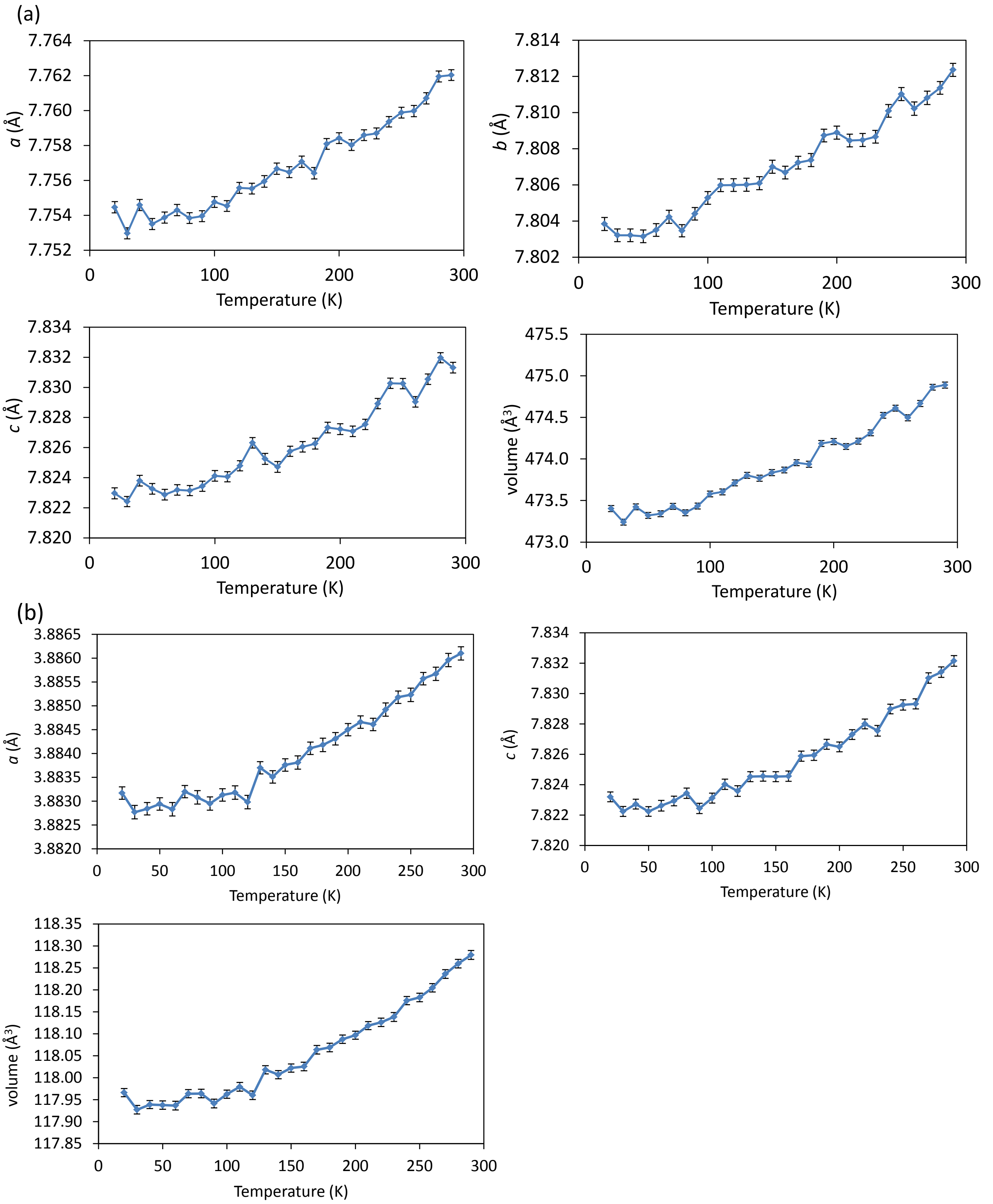

Figure SI3.2 Unit cell parameters from sequential Rietveld refinements using XRPD data collected for (a) $\mathrm{Nd}_{1/3}\mathrm{NbO}_3$ with *Cmmm* model and (b) $\mathrm{Li}_x\mathrm{Nd}_{1/3}\mathrm{NbO}_3$ with *P4/mmm* Pawley phase.

4) Density functional theory methods

The first principles calculations of the effective A^{2+} models were performed using the VASP[6-7] and ABINIT packages;[8] both employed the PBEsol[9] exchange correlation functional and PAW pseudopotentials. The plane wave cutoff was set to 1000 eV and we used a 5×5×3 *k*-point mesh for the 18 atom cell, which was scaled proportionally for other size cells.

The following details refer to the effective $A^{2+}{}_{½}NbO_3$ model. For the VASP calculations, the plane wave cutoff was set to 1000 eV, and we used a 5×5×3 *k*-point mesh for the 18 (or 20 with Li) atom cells, 7×7×3 for the 9 (or 10 atom with Li) cells, and 3×3×3 for the 36 (or 40 with Li) cells. These parameters converged the total energy, maximum force on any atom and stress to within 1 meV, 0.1 meV/ Å and 0.1 kbar, respectively. Projector Augmented Wave pseudopotentials[11] were used in the calculations with the following valence electron configuration: Be ($1s^2 2s^2$), Mg ($2s^2 2p^6 3s^2$), Ca ($3s^2 3p^6 4s^2$), Sr ($4s^2 4p^6 5s^2$), Nb ($4s^2 4p^6 5s^2 4d^3$), O ($2s^2\ 2p^4$) and Li ($1s^2 2s^1$). For the lithiated system we adopted the PBEsol+U framework as implemented by Lichtenstein et al.[12] and varied the value of U between 1 and 4 eV.

SI4.1 explicit Nd model

The first principles calculations performed on the explicit Nd models were executed with ABINIT and through the PAW approach[8] and with the PBEsol exchange-correlation functional. The phonon dispersion curves and Born effective charges were calculated through the density functional perturbation (DFPT) formalism.[13] We used the JTH (v1.1) PAW atomic data for Nb and O and we used the Nd atomic data from,[14] which was regenerated by putting the f-electrons in the core to avoid treating the strongly correlated f-electrons. We built two different cells:

(1) a 2×2×3 supercell where the Nd atoms were ordered in a rock-salt way with the empty site over 2 perovskite layers while the third layer is left with only empty *A*-sites. This model allows us to have exactly 1/3 Nd for NbO_3 stoichiometry. Even though it does not have the exact experimental structure (i.e. we have two layers with Nd instead of one experimentally for one fully *A*-site empty layer) it allows us to have the exact 1/3 concentration of Nd and thus allows to get access to the steric effect of Nd. This supercell has the *P*4/*nmm* symmetry with the atoms in the highest symmetry positions.

(2) a 1×1×2 unit cell containing one layer with fully empty *A*-site layer and one with Nd atom. Since the stoichiometry is not respected (it is $NdNb_2O_6$ in this case), we compensated the extra charge of the Nd by a background charge. This unit cell thus respects the *P*4/*mmm* symmetry and the unit cell structure observed in the experiments.

The calculations were converged with a cutoff energy for the plane wave expansion of 20 Ha (544 eV) and *k*-points grid of 3×3×2 for the 2×2×3 supercell with rock-salt arrangement of the Nd and of 8×8×6 for the 1×1×2 unit cell with the charge compensation. The relaxations were performed up to the maximum residual on forces of 8×10^{-6} Hartree/Bohr (0.0004 eV $Å^{-1}$).

While a full relaxation (cell parameters and internal atomic coordinates) could be done for the 2×2×3 supercell, only internal coordinates can be performed with a charge background compensation present in the 1×1×2 unit cell.[15] We thus used the relaxed cell parameters obtained for the 2×2×3 supercell and used it for the 1×1×2 unit cell and relaxed only the internal coordinates before running the DFPT calculations. This is justified by the fact that the cell parameters obtained in the 2×2×3 supercell are in very good agreement with the experimental results (error < 1%). With these parameters, we get a precision on the phonon frequencies of about 1 cm^{-1}.

SI4.2 the lattice parameters of the *P*4/*mmm* explicit Nd calculations

#Atom	*a*	*c*
1 Ce	3.9167	5.9330
2 Pr	3.9128	5.9202
3 Nd	3.9101	5.9099
4 Pm	3.9083	5.9012
5 Sm	3.9072	5.8941

6 Eu	3.9067	5.8880
7 Gd	3.9065	5.8819
8 Tb	3.9063	5.8763
9 Dy	3.9069	5.8720
10 Ho	3.9076	5.8677
11 Er	3.9082	5.8636
12 Tm	3.9092	5.8601
13 Yb	3.9107	5.8573
14 Lu	3.9121	5.8537

SI4.3 the phonons of the *P*4/*mmm* explicit Nd (top) compared with effective Ca (bottom) calculations

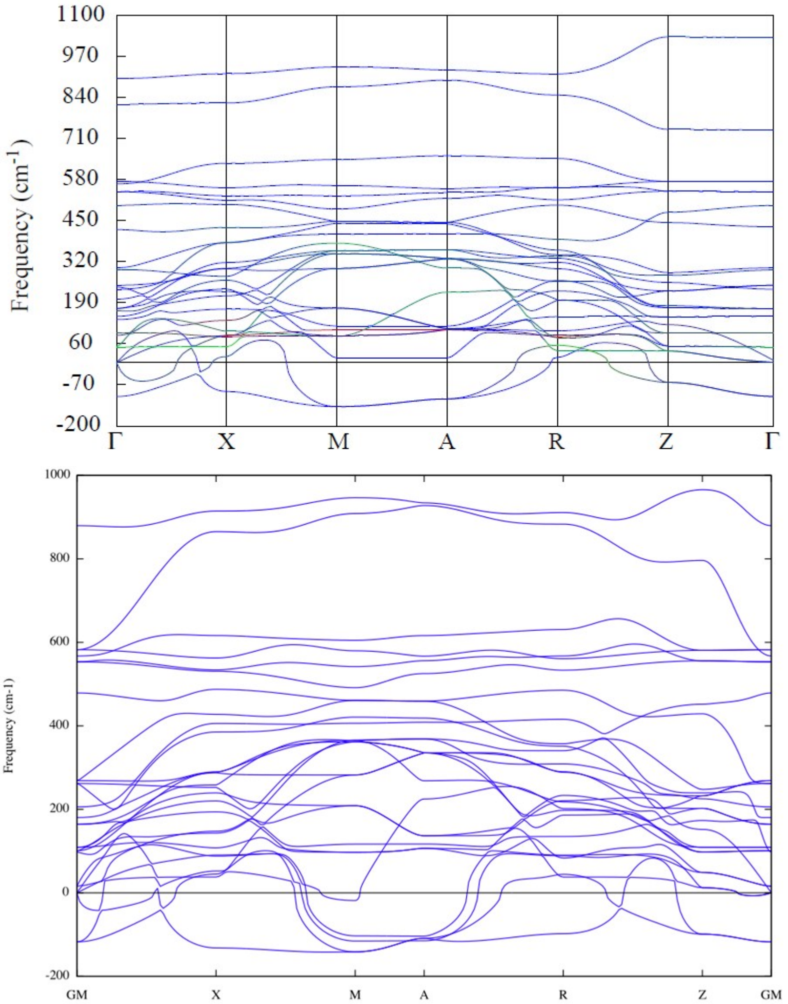

SI4.4 Table of relative energies for structural distortions for $A^{2+}_{1/2}NbO_3$ series

	Be	Mg	Ca	Sr
$a^-b^0c^0$	-3.21E+00	-8.90E-01	-1.89E-01	-1.62E-04
$a^-a^-c^0$	-3.85E+00	-1.23E+00	-1.64E-01	3.72E-04
$a^0a^0c^+$	-2.53E+00	-8.94E-01	-7.37E-02	3.91E-04
P*x*	-4.49E+00	-7.48E-01	-3.12E-02	-2.29E-03
P*xy*	-3.33E+00	-6.11E-01	-2.50E-02	-2.54E-03

5) Magnetic characterisation of $Nd_{1/3}NbO_3$ and $Li_xNd_{1/3}NbO_3$

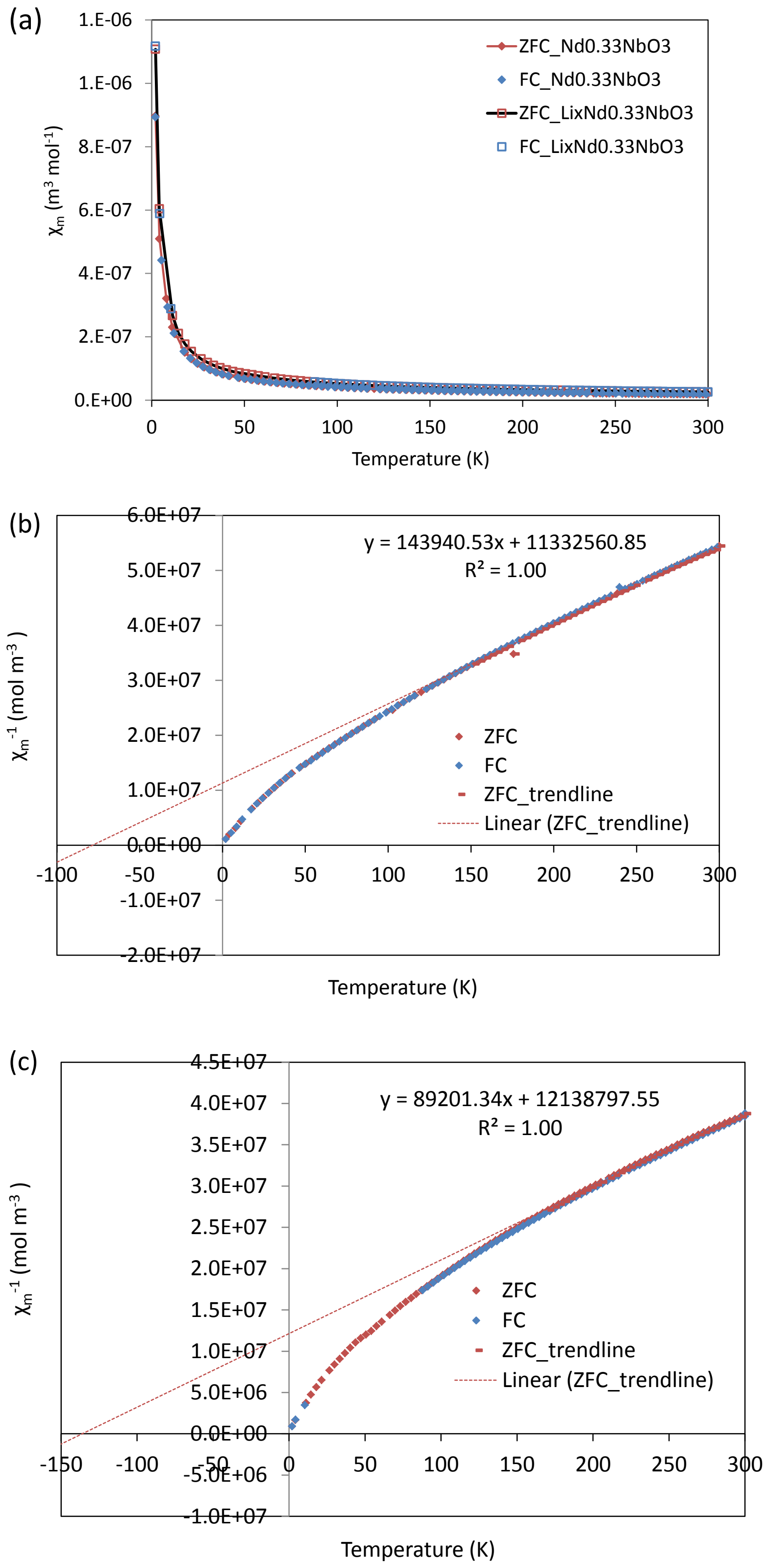

Figure SI5 (a) ZFC and FC magnetic susceptibility data for $Nd_{1/3}NbO_3$ and $Li_xNd_{1/3}NbO_3$ on warming in an applied magnetic field of 1000 Oe and Curie-Weiss analysis for (b) $Nd_{1/3}NbO_3$ (with a moment of 2.10 μ_B per formula unit and Weiss temperature θ = -79 K) and (c) $Li_xNd_{1/3}NbO_3$ (with a moment of 2.67 μ_B per formula unit and Weiss temperature θ = -136 K).

6) Neutron powder diffraction analysis of $Li_xNd_{1/3}NbO_3$

Rietveld refinement using room temperature NPD data for $Li_xNd_{⅓}NbO_3$ with *P4/mmm* model. Simulated annealing suggests a stoichiometry of Li0.31(2)Nd⅓NbO3, with Li located on both the Nd site as well as small amounts on the vacant *A* site.

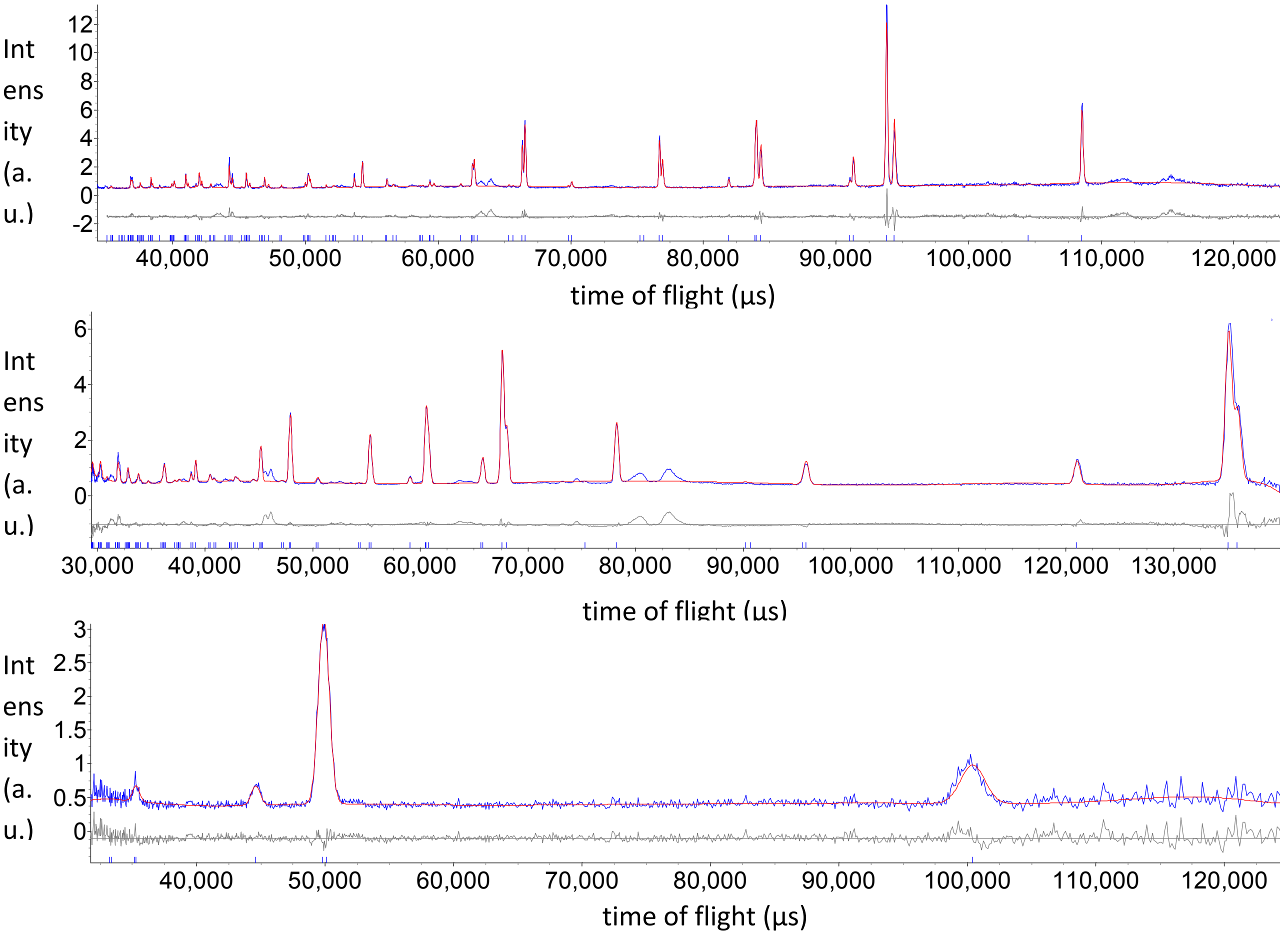

Figure SI6.1 Rietveld refinement profiles for room temperature NPD data collected for $Li_xNd_{⅓}NbO_3$ with ordered *P4/mmm* model showing observed, calculated and difference profiles in blue, red and grey, respectively, with peak positions shown by blue ticks; R_{wp} = 10.74%, R_p = 8.20% and χ^2 = 19.42. The upper panel shows the fit to the highest resolution backscattered bank, in the middle the 90° bank of data and bottom, lowest resolution 30° bank of data.

Table SI6.1 Refinement details from Rietveld refinements using room temperature NPD data collected for $Li_{0.31(2)}Nd_{⅓}NbO_3$ with ordered *P4/mmm* model with *a* = 3.8855(1) Å, *c* = 7.8198(2) Å, volume = 118.059(8) Å^3; R_{wp} = 10.74%, R_p = 8.20%, χ^2 = 19.42.

Atom	**site**	**x**	**y**	**z**	**occupancy**	**Uiso × 100 (Å^2)**
Nd/Li(1)	1c	0.5	0.5	0	0.667/0.33(4)	0.2(1)
Li(2)	2f	0.5	0	0	0.15(2)	0.2(1)
Li(3)	1d	0.5	0.5	0.5	0.21(3)	0.2(1)
Nb	2g	0	0	0.2608(3)	1	0.2(1)
O(1)	1a	0	0	0	1	-
O(2)	1b	0	0	0.5	1	-
O(3)	4i	0	0.5	0.2301(6)	1	-

	U_{ij} × 100 (Å^2)					
Atom	**U_{11}**	**U_{22}**	**U_{33}**	**U_{12}**	**U_{13}**	**U_{23}**
O(1)	15(1)	12.8(8)	3(3)	0	0.7(8)	0
O(2)	16(1)	11(1)	2.7(7)	-0.4(1)	-4.3(7)	1.7(9)
O(3)	9.0(3)	3.3(2)	13.4(4)	-0.7(2)	-1.1(5)	1(4)

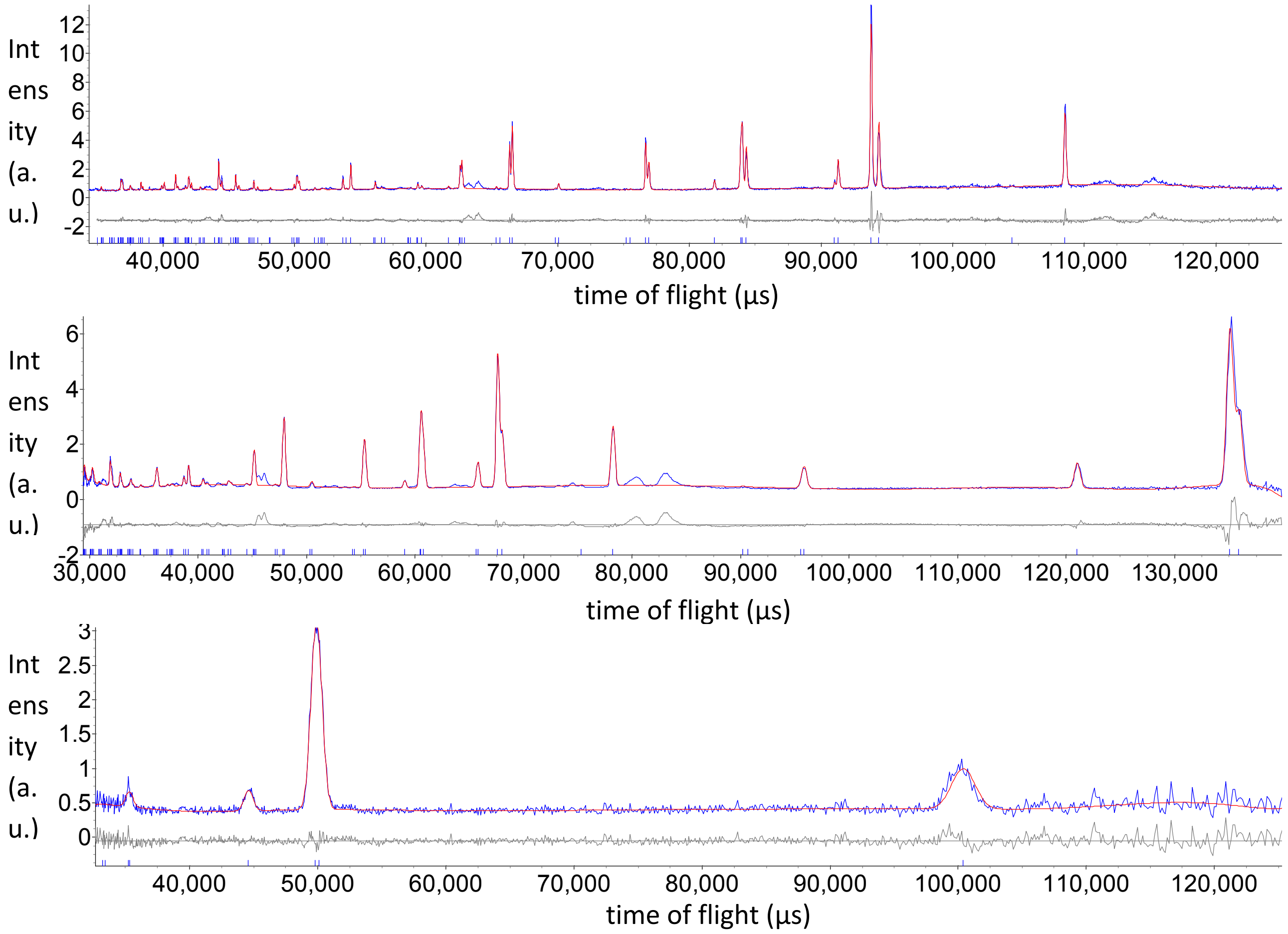

Figure SI6.2 Rietveld refinement profiles for room temperature NPD data collected for $Li_xNd_{2/3}NbO_3$ with disordered *P4/mmm* model showing observed, calculated and difference profiles in blue, red and grey, respectively, with peak positions shown by blue ticks; R_{wp} = 10.60%, R_p = 8.01%, χ^2 = 18.94. The upper panel shows the fit to the highest resolution backscattered bank, in the middle the 90° bank of data and bottom, lowest resolution 30° bank of data.

Table SI6.2 Refinement details and selected bond lengths from Rietveld refinements using room temperature NPD data collected for $Li_{0.26(2)}Nd_{2/3}NbO_3$ with disordered *P4/mmm* model with *a* = 3.8857(1) Å, *c* = 7.8200(2) Å, volume = 118.070(8) Å^3; R_{wp} = 10.60%, R_p = 8.01%, χ^2 = 18.94.

Atom	**site**	**x**	**y**	**z**	**occupancy**	**U_{iso} × 100 (Å^2)**
Nd/Li(1)	1c	0.5	0.5	0	0.667/0.33(4)	0.5(1)
Li(2)	2f	0.5	0	0	0.04(2)	0.5(1)
Li(3)	1d	0.5	0.5	0.5	0.17(2)	0.5(1)
Nb	2g	0	0	0.2611(3)	1	-
O(1)	4j	0.060(9)	0.060(9)	0	1	-
O(2)	4k	0.078(1)	0.078(1)	0.5	1	-
O(3)	4i	0	0.5	0.2294(7)	1	-

	U_{ij} × 100 (Å^2)					
Atom	**U_{11}**	**U_{22}**	**U_{33}**	**U_{12}**	**U_{13}**	**U_{23}**
Nb	0.5(3)	1.6(2)	1.0(2)	-1(1)	-0.3(2)	2.0(7)
O(1)	6(1)	5(2)	0.0(5)	-0.5(9)	1(8)	0(8)
O(2)	0.02(7)	4(1)	4.0(7)	-0.4(4)	2.6(7)	5(1)
O(3)	7.3(4)	0.1(1)	13.8(4)	0.0(2)	0.2(5)	0.0(1)

Bond	**Length (Å)**	**Bond**	**Length (Å)**
Nd/Li(1) – O(1)	1 × 2.39(4)	Nb – O(2)	1 × 1.918(4)
Nd/Li(1) – O(3)	8 × 2.645(4)	Nb – O(3)	4 × 1.9584(7)
Nd/Li(1) – O(1)	2 × 2.771(6)	Nb – O(1)	1 × 2.071(1)
Nd/Li(1) – O(1)	1 × 3.10(4)		
Li(2) – O(1)	1 × 1.71(2)	Li(3) – O(2)	1 × 2.32(1)
Li(2) – O(3)	2 × 1.795(5)	Li(3) – O(2)	2 × 2.781(1)

Li(2) – O(1)	1 × 2.21(3)	Li(3) – O(3)	8 × 2.873(4)

A LeBail refinement was carried out using the incommensurate $Ammm(0,0,g)000$ model with a = 7.8209(1) Å, 5.4954(1) Å, c = 5.4970(1) Å, q = 0 0 0.9088(2):

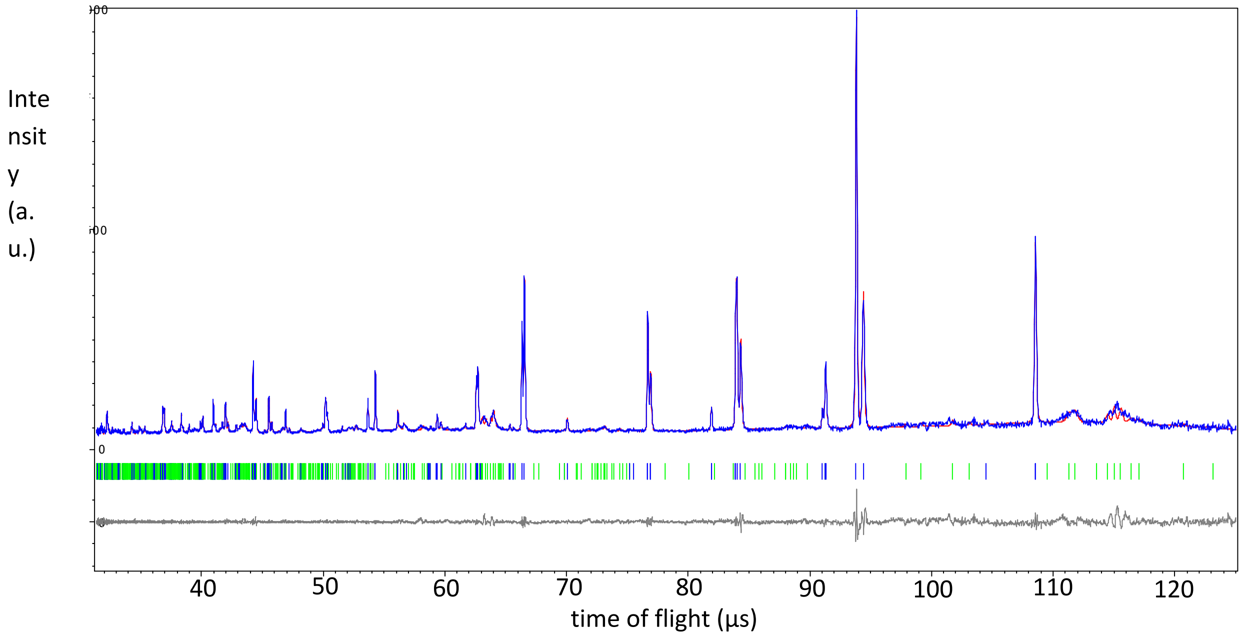
Intensity (a.u.)
0
40
50
60
70
80
90
100
110
120
time of flight (µs)

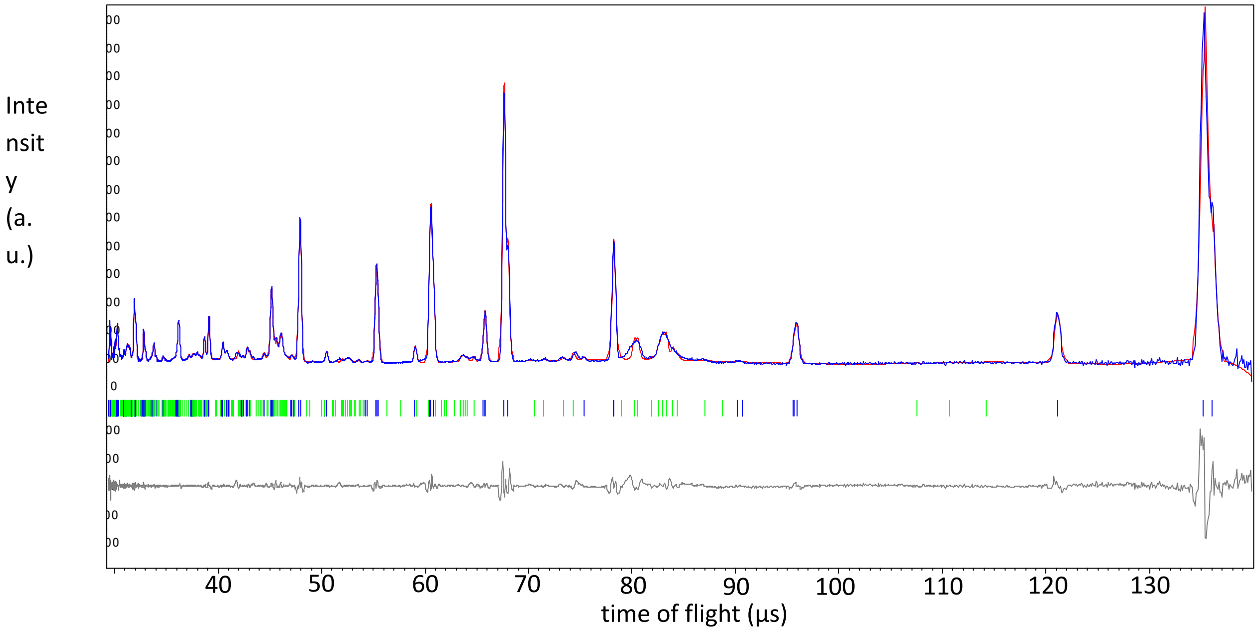
Intensity (a.u.)
0
40
50
60
70
80
90
100
110
120
130
time of flight (µs)

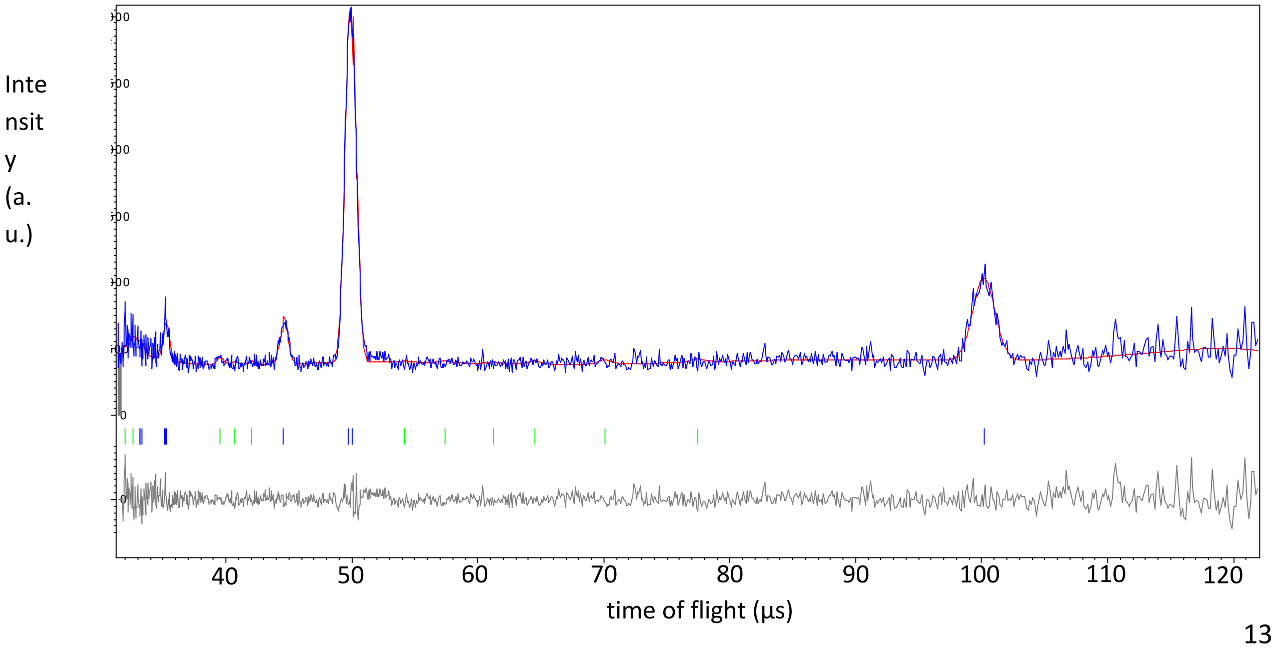
Intensity (a.u.)
0
40
50
60
70
80
90
100
110
120
time of flight (µs)

Figure SI6.2 Refinement profiles for room temperature NPD data collected for $Li_xNd_{1/3}NbO_3$, LeBail refinement profiles for a incommensurate Ammm(0,0,g)000 model with a = 7.8209(1) Å, 5.4954(1) Å, c = 5.4970(1) Å, q = 0 0 0.9088(2); Rwp = 5.45%, Rp = 5.47%, χ2 = 4.84, showing observed, calculated and difference profiles in blue, red and grey, respectively, with peak positions shown by blue ticks. The upper panel shows the fit to the highest resolution backscattered bank, in the middle the 90° bank of data and bottom, lowest resolution 30° bank of data.

1. Rietveld, H. M., *J. Appl. Cryst.* **1969,** *2*, 65.
2. Coelho, A. A., *J. Appl. Cryst.* **2003,** *36*, 86.
3. Coelho, A. A. *Topas Academic: General profile and structure analysis software for powder diffraction data*, Bruker AXS: Karlsruhe, Germany, 2012.
4. Petricek, V.; Dusek, M.; Palatinus, L., *Z. Kristallogr.* **2014,** *229* (5), 345-352.
5. Campbell, B. J.; Stokes, H. T.; Tanner, D. E.; Hatch, D. M., *J. Appl. Cryst.* **2006,** *39*, 607-614.
6. Kresse, G.; Hafner, J., *Phys. Rev. B* **1993,** *47*, 558.
7. Kresse, G.; Furthmuller, J., *Comput. Mater. Sci.* **1996,** *6*, 15.
8. Gonze, X.; Jollet, F.; Araujo, F. A.; Adams, D.; Amadon, B.; Applencourt, T.; Audouze, C.; Beuken, J.-M.; Bieder, J.; Bokhanchuk, A.; Bousquet, E.; Bruneval, F.; Caliste, D.; Cote, M.; Dham, F.; Pieve, F. d.; Delaveau, M.; Gennaro, M. d.; Dorado, B.; Espejo, C.; Geneste, G.; Genovese, L.; Gerossier, A.; Giantomassi, M.; Gillet, Y.; Harman, D. R.; He, L.; Jomard, G.; Janssne, J. L.; Roux, S. L.; Levitt, A.; Lherbier, A.; Liu, F.; Lukavcevic, I.; Martin, A.; Martins, C.; Oliveira, M. J. T.; Ponce, S.; Pouillon, Y.; Rangel, T.; Rignanese, G.-M.; Romero, A. H.; Rousseau, B.; Rubel, O.; Shukri, A. A.; Stankovski, M.; Torrent, M.; Setten, M. J. v.; Troeye, B. v.; Verstraete, M. J.; Waroquiers, D.; Wiktor, J.; Xu, B.; Zhou, A.; Zwanziger, J. W., *Comp. Phys. Commun.* **2016,** *205*, 106-131.
9. Perdew, J. P.; Ruzsinszky, A.; Csonka, G. I.; Vydrov, O. A.; Scuseria, G. E.; Constantin, L. A.; Zhou, X.; Burke, K., *Phys. Rev. Lett.* **2008,** *100*, 136406.
10. Zhou, Q.; Saines, P. J.; Sharma, N.; Ting, J.; Kennedy, B. J.; Zhang, Z.; Withers, R. L.; Wallwork, K. S., *Chem. Mater.* **2008,** *20*, 6666-6676.
11. Blochl, P. E., *Phys. Rev. B* **1994,** *50*, 17953.
12. Liechtenstein, A. I.; Anisimov, V. I.; Zaanen, J., *Phys. Rev. B* **1995,** *52*, R5467.
13. Gonze, X.; Lee, C., *Phys. Rev. B* **1997,** *55*, 10355.
14. Topsakal, M.; Wentzcovitch, R. M., *Comp. Mater. Sci.* **2014,** *95*, 263-270.
15. Bruneval, F.; Varvenne, C.; Crocombette, J.-P.; Clouet, E., *Phys. Rev. B* **2015,** *91*, 024107.